

Modeling Soil: Realtime Dynamic Models for Soil Slippage and Manipulation

Xin Li and J. Michael Moshell

Institute for Simulation and Training
University of Central Florida

ABSTRACT

A physically based model of an object is a mathematical representation of its behavior, which incorporates principles of Newtonian physics. Dynamic soil models are required in animations and realtime interactive simulations in which changes of natural terrain are involved. Analytic methods, based on soil properties and Newtonian physics, are presented in the paper to model soil slippage and soil manipulations. These methods can be used to calculate the evolution of a given soil configuration under the constraint of volume conservation and to simulate excavating activities such as digging, cutting, piling, carrying or dumping soil. Numerical algorithms with linear time and space complexities are also developed to meet the requirement of realtime computer simulation.

CR Categories: I.3.7 [Computer Graphics]: Graphics and Realism; I.6.3 [Simulation and Modeling]: applications.

Additional Keywords: physically based modeling, realtime simulation, soil dynamics, slippage, soil manipulation.

1. INTRODUCTION

Physically-based modeling is a growing area of computer graphics research. A good deal of work has been done toward physically based models of objects such as rigid and nonrigid bodies, hydraulic surfaces or natural terrain. However, soil models that are both physically realistic and computationally efficient in realtime simulations have not been developed. Recently, substantial interest in dynamic soil models has been expressed by some developers of realtime simulations of Dynamic Terrain systems. Such systems provide the capability, within a realtime graphical simulation, of reconstructing landscape architecture or rearranging the terrain surface. These systems essentially involve allowing the simulation's user to conduct excavating activities in the terrain database at any freely chosen location. These activities may include digging ditches, piling up dirt, cutting the soil mass from the ground, carrying it for a distance, and dumping it at another location. To these deformations, the soil mass must behave in realistic manners under external stimuli.

Moshell and Li developed a visually plausible kinematic soil model [10]. In their work, a bulldozer blade serves as a local force function used to change the heights of the terrain. Excess terrain volume which is "scaped off" by the moving

blade is added to the moving berm in front of the blade. The berm is then smoothed by a bidirectional Cardinal spline algorithm. The demonstration of the model appears realistic and runs in realtime. The simulation, however, is kinematic. No forces are computed. The soil does not slump when the bulldozer leaves. The volume of given soil is not conserved.

Burg and Moshell focussed on the problem of piling up soil such that the soil spills down from the mounds in a realistic-looking way [3]. In their approach, the terrain is modeled by a 2-d grid of altitude posts. Constraint equations are defined to describe relationships among altitude posts and their neighbors. An iterative relaxation algorithm, suggested in [11], is used to simulate the falling soil. The constraints enforce an averaging or "smoothing" of each altitude post with its neighbors. The algorithm is volume-preserving under certain conditions. The model is purely kinematic. The physical properties of different types of soil are not modeled.

Our research work is focused on dynamic models of soil slippage and soil manipulations. For the slippage model, we determine if a given soil configuration is in static equilibrium, calculate forces which drive a portion of the soil to slide if the configuration is not stable, and meanwhile preserve the volume conservation. For the soil manipulation models, we investigate interactions between soil and excavating machines, implement a bulldozer model and a scooploader model. These models are based on analytic methods and Newtonian physics. The computational times of the corresponding algorithms are fast enough to meet the requirement of realtime graphical simulations. For clarity, this paper mainly focuses on the 2-d case. Extensions to 3-d have been completed and are briefly discussed.

2. PRELIMINARIES

The discussion of soil models needs some understanding of soil properties. In this section, we introduce some concepts which are borrowed directly from civil engineering. Interested readers are referred to [2], [4], [5] and [7] for more details.

The *shear strength* of the soil is the resistance per unit area to deformation by continuous shear displacement of soil particles along surfaces of rupture. It may be attributed to three basic components: 1) frictional resistance to sliding among soil particles; 2) cohesion and adhesion among soil particles; and 3) interlocking of solid particles to resist deformation. (Cohesion is molecular attraction among like particles. Adhesion is a molecular attraction among unlike particles.)

The *shear stress*, on the other hand, is the force per unit area experienced by a slope, which pushes the mass to move along the failure plane. The combined effects of gravity and water are the primary influences on the shear stress. It may also be influenced by some natural phenomena such as chemical actions, earthquakes, or wind.

The *shear strength force* and *stress force*, denoted by s and τ respectively, are defined as the shear strength and stress

12424 Research Parkway, Suite 300, Orlando, Florida.
Phone: (407) 658-5073, email: lix@ist.ucf.edu

This work is sponsored by the U.S. Army Simulation, Training and Instrumentation Command (STRICOM). All opinions are, however, solely due to the authors.

multiplied by the total area. The measure of s and τ can be determined from the *Mohr-Coulomb theory* indicated in [5]:

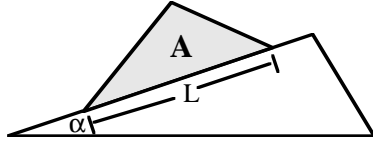


Fig. 1: The Failure Plane

$$(2.1) \quad s = c L + W \cos(\alpha) \tan(\phi)$$

$$(2.2) \quad \tau = W \sin(\alpha)$$

where L is the length of the failure plane, α is the degree of natural slope, and $W = \gamma A$ is the weight of soil above the failure plane (see Fig. 1). c , ϕ and γ describe properties of the soil, where c indicates the cohesion, ϕ is the angle of internal friction (i.e. it is a measure of the friction among soil particles) and γ is the unit weight. Some typical parameters and their units are listed in the table below [1]:

SOIL TYPE	c (t/m)	ϕ (degree)	γ (t/m ²)
dry sand	0	26-33	1.9-2.0
Sandy loam	0-2.0	14-26	1.8-2.0
Loam	0.5-5.0	10-28	1.8-2.1

Soil is a very complex material. It may be influenced by changes in the moisture content, pore pressures, structural disturbance, fluctuation in the ground water table, underground water movements, stress history, time, chemical action or environmental conditions. Predicting the changes of complex configurations is either intractable or highly costly. However, for many interactive applications, speed and realistic appearance are more important than accuracy. Hence in this paper, we assume that only homogeneous and isotropic soil will be processed. Conditions such as seepage, pore pressure, existence of tension cracks and deformation resulting from permanent atomic dislocation will not be considered.

3. STATIC EQUILIBRIUM AND RESTORING FORCE

In this section, we develop methods to determine whether or not a given configuration is stable, calculate the critical angle above which sliding occurs, and quantify the force which pushes the soil mass moving along the failure plane.

3.1 STABILITY

The stability of a given soil configuration is determined by the *factor of safety*, denoted by F , of a potential failure surface. From the Mohr-Coulomb theory, F is defined as a ratio between the strength force and the stress force [5]:

$$(3.1) \quad F = \frac{s}{\tau} = \frac{c L + W \cos(\alpha) \tan(\phi)}{W \sin(\alpha)}$$

When F is greater than 1, the configuration is said to be in a state of equilibrium. Otherwise, failure is imminent. To analyze the factor of safety, we divide the given soil mass into n slices with equal width Δx :

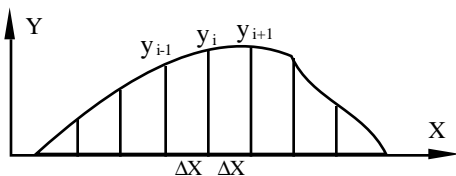


Fig. 2: Dividing the given mass into small slices

The calculation of the factor of safety of each slice can be done individually. The following free body diagram shows forces applied on slice i :

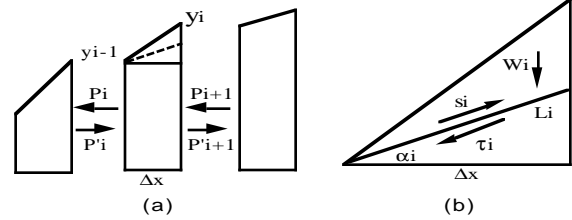


Fig. 3: Free body diagram for slice i

In (a), the P 's are forces exerted between slices. They are pairwise equal and in opposite directions and thus can be cancelled. At any time t , therefore, sliding can only happen in the top triangle area of a slice. (b) shows forces acting on this area, where strength and stress forces are given by (2.1) and (2.2) with L , W and α replaced by L_i , W_i and α_i respectively.

To determine if there exists a failure angle α_i (so that the soil mass above it will slide) and calculate the net force exerted on the failure plane if α_i does exist, we start from (3.1). Note that L_i and W_i can be expressed in terms of α_i . Replacing L_i and W_i in (3.1) with functions of α_i , we obtain

$$(3.2) \quad F(\alpha_i) = \frac{2c + \gamma \tan(\phi) [h \cos(\alpha_i) - \Delta x \sin(\alpha_i)] \cos(\alpha_i)}{\gamma (h \cos(\alpha_i) - \Delta x \sin(\alpha_i)) \sin(\alpha_i)}$$

where $h = y_i - y_{i-1}$ is the height of the triangle in Fig. 3-(b). For any angle $\alpha_i > \tan^{-1}(h/\Delta x)$, function $F(\alpha_i)$ makes no physical sense. In the range of $[0, \tan^{-1}(h/\Delta x)]$, $F(\alpha_i)$ reaches its minimum when the first derivative of $F(\alpha_i)$, with respect to α_i , is equal to 0. That is

$$(3.3) \quad \frac{dF}{d\alpha} = \frac{1}{\tau^2} [A \cos(2\alpha_i) + B \sin(2\alpha_i) + C] = 0$$

where

$$A = \frac{\gamma^2}{2} \tan(\phi) (\Delta x^2 - h^2) - 2\gamma c h,$$

$$B = \gamma^2 h \Delta x \tan(\phi) + 2\gamma c \Delta x, \text{ and}$$

$$C = -\frac{\gamma^2}{2} \tan(\phi) (\Delta x^2 + h^2).$$

Solving (3.3) gives us four angles (see [9]). We can choose the one which satisfies $0 \leq \alpha_i \leq \tan^{-1}(h/\Delta x)$ in (3.2) to calculate the factor of safety F . The given configuration is statically stable if $F > 1$. Otherwise sliding is inevitable.

3.2 CRITICAL SLOPE ANGLE

Suppose that we have $F < 1$ for a given configuration. In the range of $[0, \tan^{-1}(h/\Delta x)]$ there are at most two angles, say β_1 and β_2 , such that $F(\beta_1) = F(\beta_2) = 1$. The angle $\beta_0 = \min(\beta_1, \beta_2)$ is said to be the *critical-slope angle* of the configuration. Above this angle impending slip occurs. β_1 and β_2 can be obtained by solving the equation (3.4) for α :

$$(3.4) \quad F(\alpha) = \frac{2c + \gamma \tan(\phi) [h \cos(\alpha) - \Delta x \sin(\alpha)] \cos(\alpha)}{\gamma (h \cos(\alpha) - \Delta x \sin(\alpha)) \sin(\alpha)} = 1$$

where all symbols are as explained earlier. The solution to (3.4) is derived in [9].

3.3 RESTORING FORCE

Let a configuration be given in Fig.4-(a) with β_0 as the critical-slope angle. The force that pushes the mass in the triangle along the edge gh_0 can be computed as follows. First the line segment h_0h_n is divided into n small segments with equal length Δh . Fig 4-(b) shows the free body diagram of the i -th dovetail indicated by the shaded area in (a).

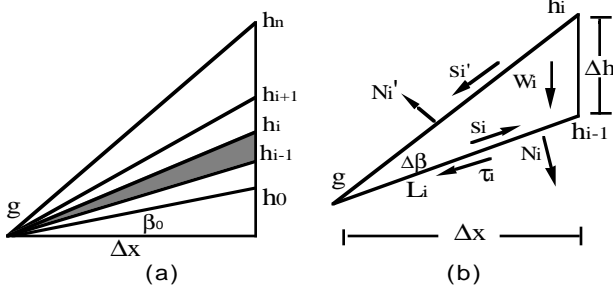


Fig. 4: Analyzing the restoring force

Let's analyze forces exerted on the dovetail. The weight W_i can be decomposed into two forces, namely N_i and τ_i , which are normal and parallel to the edge L_i respectively. s_i is the strength force resisting the sliding motion, s_i' the opponent force generated by strength force s_{i+1} , and N_i' the force supporting the dovetail above it. The net force f_i applied on dovetail- i is therefore given by a vectorial summation:

$$(3.5) \quad f_i = N_i + \tau_i + s_i + s_i' + N_i'$$

The total net force f acting on the whole triangle area is the summation of f_i 's, $1 \leq i \leq n$, i.e.

$$(3.6) \quad f = \sum_{i=1}^n (N_i + \tau_i + s_i + s_i' + N_i') = \sum_{i=2}^n \tau_i$$

since $\tau_1 = s_1$ (due to $F(\beta_0) = 1$), $N_n' = 0$, $s_n' = 0$, $N_i' = N_{i+1}$ and $s_i' = -s_{i+1}$ for $1 \leq i \leq n-1$. Based on (3.6) and Fig.4, [9] gives a derivation of (3.7) by letting Δh tend to zero.

$$(3.7) \quad f = \frac{\gamma \Delta x^2}{4} \text{Ln} \left(\frac{h_n^2 + \Delta x^2}{h_0^2 + \Delta x^2} \right) \cos(\beta_0) + \frac{\gamma \Delta x}{2} (h_n - h_0 - \Delta x(\beta_n - \beta_0)) \sin(\beta_0)$$

where $\beta_n = \tan^{-1}(h_n/\Delta x)$ and $\beta_0 = \tan^{-1}(h_0/\Delta x)$. (3.7) can be used to quantify the total force on the top triangle area of each slice.

4. VOLUME CONSERVATION

The approach used in this section is strongly related to [8]. Recall that, in the previous discussion, a given configuration is divided into n slices. The i -th slice, $1 \leq i \leq n$, can be conveniently thought of as a container holding an amount of soil whose quantity is given by $(y_i + y_{i-1})\Delta x/2$.

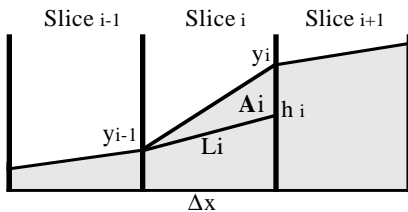


Fig. 5: Considering slices as containers

Let us consider a small change, denoted by ΔW_i , of the mass W_i in slice i . Since $W_i = (y_i + y_{i-1})\gamma \Delta x/2$, we have

$$(4.1) \quad \Delta W_i = (y_i + \Delta y_i + y_{i-1} + \Delta y_{i-1})\gamma \Delta x/2 - (y_i + y_{i-1})\gamma \Delta x/2 = (\Delta y_i + \Delta y_{i-1})\gamma \Delta x/2$$

On the other hand, let us assume that there is a force f_i exerted on the triangle area A_i at the top of slice i , which is parallel to the edge L_i . Due to f_i , A_i tends to move along the direction of f_i at a velocity v_i . The rate of the "flow" of mass of A_i through slice i can be computed by $\gamma A_i v_i / \Delta x$. Thus, the "mass throughput" of slice i can be quantified by $\gamma A_i v_i \Delta t / \Delta x$, where Δt is a unit of time. Similarly, the mass throughput of slice $i+1$ is given by $\gamma A_{i+1} v_{i+1} \Delta t / \Delta x$.

From the principle of volume conservation, the change of soil quantity in slice i is the amount of soil which goes out, minus the amount of soil which goes in. It can be expressed by

$$(4.2) \quad \Delta W_i = \frac{\gamma A_i}{\Delta x} v_i \Delta t - \frac{\gamma A_{i+1}}{\Delta x v_{i+1}} \Delta t$$

where $A_i = (y_i - h_i)\Delta x/2$. Putting (4.1) and (4.2) together and rearranging it, we have

$$(4.3) \quad \frac{\Delta y_i}{\Delta t} + \frac{\Delta y_{i-1}}{\Delta t} = \frac{1}{\Delta x} [(y_i - h_i)v_i - (y_{i+1} - h_{i+1})v_{i+1}]$$

Now let Δt tend to 0. It follows that

$$(4.4) \quad \frac{dy_i}{dt} + \frac{dy_{i-1}}{dt} = \frac{1}{\Delta x} [(y_i - h_i)v_i - (y_{i+1} - h_{i+1})v_{i+1}]$$

Recall that (3.7) gives us a formula to compute force f_i . From Newton's second law, we have

$$(4.5) \quad f_i = \gamma A_i \frac{dv_i}{dt} = \frac{\gamma \Delta x}{2} (y_i - h_i) \frac{dv_i}{dt}$$

Rearranging, we obtain both

$$(4.6) \quad \frac{dv_i}{dt} = \frac{2f_i}{\gamma \Delta x (y_i - h_i)}, \text{ and}$$

$$(4.7) \quad v_i = \frac{2}{\gamma \Delta x} \int \frac{f_i}{y_i - h_i} dt$$

Now we take the second derivative of (4.4) with respect to t and plug (4.6) and (4.7) into the resulting formula. That yields

$$(4.8) \quad \frac{d^2 y_i}{dt^2} + \frac{d^2 y_{i-1}}{dt^2} = \frac{2}{\gamma \Delta x} \left[\frac{dy_i - dh_i}{dt} \int \frac{f_i}{y_i - h_i} dt + f_i - \frac{dy_{i+1} - dh_{i+1}}{dt} \int \frac{f_{i+1}}{y_{i+1} - h_{i+1}} dt + f_{i+1} \right]$$

Note that we can denote h_i and f_i as functions of y_{i-1} and y_i , i.e. $h_i = h(y_{i-1}, y_i)$ and $f_i = f(y_{i-1}, y_i)$, since they can be determined based only on y_{i-1} and y_i if Δx and other soil properties are fixed. Hence, (4.8) is an equation with three variables, namely y_{i-1} , y_i , y_{i+1} . Let us suppose that we have divided the given configuration into n slices. Now we end up with $n+1$ unknowns, y_0, y_1, \dots, y_n , and $n+1$ ordinary differential equations involving y_i 's, their time derivatives and integrals. Solving these equations, we will obtain the solution for the soil behavior which satisfies both the soil dynamics and the volume conservation.

5. NUMERICAL SOLUTION

In this section we linearize equations (4.8) for both purposes of simplification and discretization. we start from (4.4). Assume that, at any instance of time t_m , velocity v_i of the mass on the top of slice _{i} is represented by $v_i(t_m)$, the value of y_i is represented by $y_i(t_m)$, the rate of the change of y_i is represented by $y_i'(t_m)=dy_i(t_m)/dt$. Then, at the very next time instance t_{m+1} , the force $f_i=f_i(y_{i-1}(t_m), y_i(t_m))$ can be computed by (3.7) according to the value of y_{i-1} and y_i from the previous step. If the Euler integration algorithm is used, the velocity v_i at the time t_{m+1} can be computed by

$$(5.1) \quad v_i(t_{m+1}) = v_i(t_m) + \frac{f_i(y_{i-1}(t_m), y_i(t_m))}{W_i} \Delta t$$

where Δt is the integration step size. Similarly $v_{i+1}(t_{m+1})$ is calculated. It follows that, from (4.5), we have

$$(5.2) \quad y_i'(t_{m+1}) + y_{i-1}'(t_{m+1}) = \frac{1}{\Delta x} [(y_i(t_m) - h(y_{i-1}(t_m), y_i(t_m)))v_i(t_{m+1}) - (y_{i+1}(t_m) - h(y_i(t_m), y_{i+1}(t_m)))v_{i+1}(t_{m+1})]$$

Since at the time instance t_{m+1} , all items on the right hand side are knowns, either from the previous step of the simulation or from the calculations of $v_i(t_{m+1})$ and $v_{i+1}(t_{m+1})$, we may treat it as a constant, namely C_i . We now have $n+1$ equations in the following format:

$$(5.3) \quad \begin{aligned} y_0'(t_{m+1}) &= C_0 \\ y_1'(t_{m+1}) + y_0'(t_{m+1}) &= C_1 \\ &\dots\dots \\ y_n'(t_{m+1}) + y_{n-1}'(t_{m+1}) &= C_n \end{aligned}$$

Solving (5.3) for $y_i'(t_{m+1})$, $i=0, 1, \dots, n$, we will be able to use the Euler method again to determine the new values for each y_i :

$$(5.4) \quad y_i(t_{m+1}) = y_i(t_m) + y_i'(t_{m+1})\Delta t$$

Algorithm 1 describes the procedure of the numerical solution, in which each step of the algorithm takes linear time to execute. Thus the time complexity of the algorithm is $O(n)$ where n is the number of elevation posts in a given configuration. The space required to store forces, velocities and heights of posts is also proportional to n .

Algorithm 1.

At any time t_{m+1} of simulation, do the following:

- 1) for each post y_i , calculate its mass velocity $v_i(t_{m+1})$ by using (5.1);
- 2) for y_i , compute the right hand side of (5.2);
- 3) use forward substitution to solve equations (5.3) for $y_i'(t_{m+1})$, $i=0, 1, \dots, n$;
- 4) use Euler integration to determine new value for each $y_i(t_{m+1})$.

6. EXTENSION TO 3-D

In going to 3-d soil dynamics, we use some essential concepts and results from the discussion on 2-d. First, a given soil configuration is partitioned into small prisms. The values of elevation posts (i.e. vertices) of each prism are evolved by an approximation procedure as follows.

Consider, in Fig. 6, the post $z(i,j)$ chosen arbitrarily:

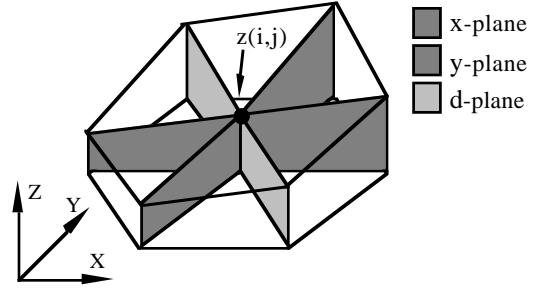


Fig. 6: An approximation of the 3-d configuration

$z(i, j)$ is surrounded by six prisms. At any time instance t , those prisms are the only ones that affect the height of $z(i,j)$. The effect caused by those prisms can be approximated by considering forces exerted on three planes, namely the x-plane, y-plane and d-plane. They are indicated by different types of shaded areas in Fig. 6. Thus the 3-d problem is reduced to a 2-d problem. The finer the partitioning is, the smaller the base triangles of prisms are, and the more accurate the approximation will be.

Let's assume that, at any time t_m , the height of post $z(i,j)$ is represented by $z_{ij}(t_m)$, and the rate of change of $z(i,j)$ is represented by $z_{ij}'(t_m)$. Since $z_{ij}'(t_m)$ is affected by forces from 3 planes, it can be expressed as a summation of three terms:

$$(6.1) \quad z_{ij}'(t_m) = zx_{ij}'(t_m) + zy_{ij}'(t_m) + zd_{ij}'(t_m)$$

where $zx_{ij}'(t_m)$, $zy_{ij}'(t_m)$ and $zd_{ij}'(t_m)$, are rates of changes of $z_{ij}'(t_m)$ caused by forces exerted on the x-plane, y-plane and d-plane respectively.

During a simulation, each time slice Δt is divided into two substeps Δt_1 and Δt_2 . In Δt_1 , we first use (3.7) to compute forces exerted on three different planes. Then $zx_{ij}'(t_{m+1})$, $zy_{ij}'(t_{m+1})$ and $zd_{ij}'(t_{m+1})$ can be obtained by solving equations (5.3). In step Δt_2 , Euler integration is used to determine new values for each $z_{ij}(t_{m+1})$:

$$(6.2) \quad z_{ij}(t_{m+1}) = z_{ij}(t_m) + [zx_{ij}'(t_m) + zy_{ij}'(t_m) + zd_{ij}'(t_m)]\Delta t$$

For Δt_1 and Δt_2 of each iteration in the simulation, we split our 2-d computational problem into 3 terms: x-plane scan, y-plane scan and d-plane scan. Each scan has two phases corresponding to two time substeps. A scan on any plane involves calculations of forces exerted on that plane, rates of changes of $z(i, j)$ caused by the forces, new height of each post, etc. Computations for each scan in a time substep are independent of scans on the other planes in the same substep, and therefore can be performed either sequentially or in parallel. It is important to notice that, in the same time substep, scans in different orders (x-scan then y-scan then d-scan, or y-scan then x-scan then d-scan, etc.) will have the same effect. The reasons are discussed in [9].

The 3-d algorithm can be briefly described as follows: Each iteration of simulation is divided into two phases. Steps (1)-(3) of Algorithm 1 are performed first for each scan. Then step (4) is applied for each scan to calculate new values of posts. Both time and space complexity of the 3-d algorithm remain linear in the number of posts.

7. INTERACTION BETWEEN SOIL AND BLADE

In this section, we analyze the interaction between the soil mass and a bulldozer's blade. Let's assume that the height of the blade is H . The shape of the blade can be modeled by an arc of a circle centered at the location $\langle x_c, y_c \rangle$ with radius R . We divide the arc into n segments, each of which has length $R\Delta\beta$. Furthermore, the soil mass in front of the blade is also partitioned into n slices by horizontal lines at each joint point of two arc segments as shown in Fig. 7.

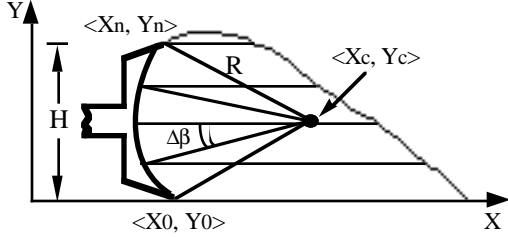


Fig. 7: Dividing the blade and soil mass

To calculate the force resisting cutting, we arbitrarily pick the i -th slice from the partitioning. The arc segment can be approximated by a line segment from point $\langle x_i, y_i \rangle$ to point $\langle x_{i+1}, y_{i+1} \rangle$. Note that the length of the line segment, denoted by ΔL , approaches the length of the arc when $\Delta\beta$ approaches 0. The idea is explained in Fig. 8:

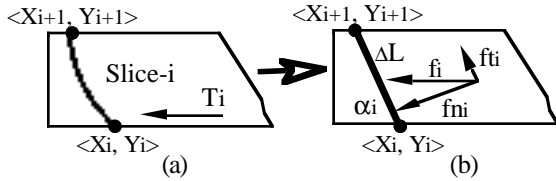


Fig. 8: Free body diagram for i -th slice

If the cutting part of the bulldozer pushes the soil mass with enough force, the equilibrium will be destroyed. At this moment, the resistance parallel to blade motion at the point $\langle x_i, y_i \rangle$ can be calculated by the formula [1]:

$$(7.1) \quad T_i = Ae^{2\alpha_i + B} [\gamma(H + y_0 - y_i) + c \cot(\phi)] \tan(\phi)$$

where T_i is the localized shear stress and α_i is the magnitude of the angle of inclination of ΔL to the horizon. The remaining symbols are as explained earlier. All angles are given in radians. Constants A and B are only related to ϕ and δ (δ is the angle of external friction), of the given soil:

$$(7.2) \quad A = \frac{\sin(\delta) [\cos(\delta) + \sqrt{\sin^2(\phi) - \sin^2(\delta)}]}{1 - \sin(\phi)}$$

$$(7.3) \quad B = \delta + \sin^{-1} \left(\frac{\sin(\delta)}{\sin(\phi)} \right) - \pi$$

Due to different cutting depths (given by $H + y_0 - y_i$) and different inclination angles α_i , the magnitudes of T_i vary. The resistance force exerted on ΔL can be computed by $f_i = T_i \Delta L$. As shown in Fig. 8-(b), f_i can be further decomposed into two components, one normal to ΔL and another parallel to ΔL . The normal force is cancelled by the opposite force contributed by ΔL . The parallel force has the following property: In the upper

portion of the blade, it has a smaller magnitude and points in the negative y -direction. In the lower portion, it has a larger magnitude and points in the positive y -direction. Let f_{y_i} be the y component of the parallel force. It can be computed by:

$$(7.4) \quad f_{y_i} = (C_1 - C_2 y_i) e^{2\alpha_i} \sin(\alpha_i) \cos(\alpha_i) \Delta L$$

where $C_1 = Ae^B [\gamma(H + y_0) \tan(\phi) + c]$ and $C_2 = Ae^B \gamma \tan(\phi)$.

Now we calculate the summation of all f_{y_i} 's, represented by F^y , which gives us the total force pushing the soil mass in front of the blade upwards.

$$(7.5) \quad F^y = \frac{1}{2} \sum_{i=1}^n (C_1 - C_2 y_i) e^{2\alpha_i} \sin(2\alpha_i) \Delta L$$

To get an accurate solution, we let $\Delta\alpha$ approach 0. In this case we have the following equations [9]:

$$(7.6) \quad \alpha_i = \alpha_0 + i \Delta\alpha$$

$$(7.7) \quad \lim_{\Delta\alpha \rightarrow 0} \Delta L = R \Delta\alpha$$

$$(7.8) \quad \lim_{\Delta\alpha \rightarrow 0} y_i = y_c - R \cos(\alpha_0 + i \Delta\alpha)$$

Replacing α_i , ΔL and y_i in (7.5) by right hand sides of above equations and making $\Delta\alpha$ infinitesimal, we obtain:

$$(7.9) \quad F^y = \frac{R}{2} \int_{\alpha_0}^{\alpha_n} [C_1 - C_2 y_c + C_2 R \cos(\alpha)] e^{2\alpha} \sin(2\alpha) d\alpha$$

To simulate cases in which the blade are not fully loaded, we fix the lower bound angle of the definite integral and keep the upper bound angle changing from α_0 to α_n . That will give us the following figure:

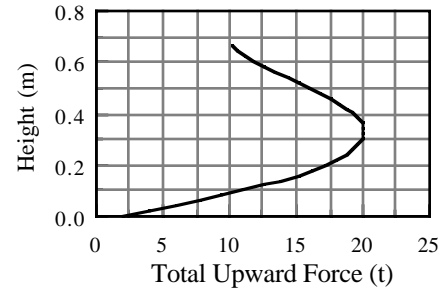


Fig. 9: Total upward force along the blade

In Fig 9, the vertical axis indicates y coordinates of points up to which the soil is loaded and the horizontal axis gives F^y under the given configuration. The data is recorded with $\alpha_0 = 1.22$, $R = 100$ cm, $c = 1.9$, $\delta = 0.5$, $\phi = 0.54$ and $\gamma = 2.0$ (angles are measured in radians). For example, if the soil is loaded up to the middle point of the height of the blade, i.e. $y = 36.0$ cm, the curve shows that at this point the total upward force reaches its maximum (about 20 metric tons).

The analysis shows that the total force is always positive. That is, the soil mass being cut always moves upward along the blade. This phenomenon is also observed experimentally [1]. The sequence of events occurring during the process of interaction between the cutting blade and the excavated soil before the blade can be described by 3 steps. 1) the soil chip being cut from the main soil mass moves upward along the

blade because of resistance to the soil. 2) the soil chip is broken up into individual lumps on the upper part of the blade. 3) These lumps move downward toward the soil layers being further cut and from the soil prism which is being dragged. This phenomenon is depicted by Fig. 10:



Fig. 10: Pattern of soil movement ahead of the blade

8. SOIL IN A BUCKET

In this section, we present a graphical model of a scooploader. For clarity, we assume that only buckets which can be represented by convex polygons will be processed. Again we first divide the soil configuration and the bucket into n slices with equal width Δx . This is shown in Fig 11, where the thick line segments indicate the bucket:

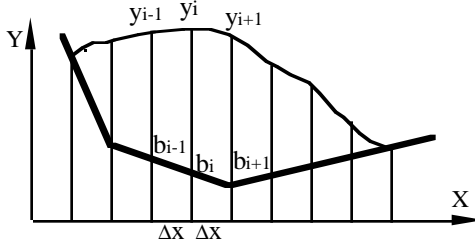


Fig. 11: Dividing the soil mass in a bucket

The motion of the soil mass in the bucket is a combination of two movements: 1) the movement of a portion of the given soil mass along a potential failure plane on the top; and 2) the whole mass along the bucket surface. We will refer to these motions as *local movement* and *global movement* respectively. In general, a local movement is caused by an unstable configuration of the given soil, while a global movement is due to the shear stress experienced by a surface of the soil mass in contact with the bucket. This can be seen more clearly through the free body diagram of slice- i arbitrarily picked from the partitioning (see Fig. 12), where f_i is the force driving a local movement along the failure plane denoted by line segment $\langle y_{i-1}, h_i \rangle$. This force can be quantified by (3.7).

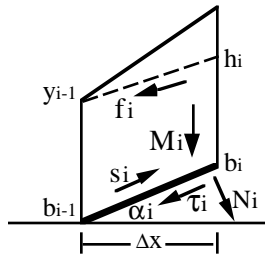


Fig. 12: Analyzing forces of slice- i

Let's now consider the global movement. The driving force, denoted by G , can be calculated by analyzing the free body diagram of each free body. As shown in Fig. 12, the weight M_i of slice- i can be decomposed into two elements: the

shear stress force τ_i and the normal stress force N_i . N_i is canceled by the opposite force provided by the bucket surface $\langle b_{i-1}, b_i \rangle$. τ_i is the force which pushes the mass to move along the bucket surface. The shear strength force s_i , on the other hand, resists the shear displacement of soil particles along the bucket surface. These forces can be determined from the Mohr-Coulomb theory as indicated by [5]:

$$(8.1) \quad \tau_i = M_i \sin(\alpha_i)$$

$$(8.2) \quad s_i = cL_i + M_i \cos(\alpha_i) \tan(\delta)$$

where c is the coefficient of cohesion, δ is the angle of external friction, L_i is the length of the line segment from b_{i-1} to b_i , M_i is the weight of slice- i , and α_i is the angle between the bucket surface and the horizontal. δ indicates a measure of the friction between soil and the surface of the bucket. It is given in radians. For loamy clay and sand, the typical values of δ are 18 and 30 respectively [1]. The units of these symbols are as explained earlier.

For equilibrium consideration, we use a method similar to the one described in [6]. The stress force τ and the strength force s can be expressed by vectorial summations:

$$(8.3) \quad \tau = \sum_{i=1}^n \tau_i = \sum_{i=1}^n M_i \sin(\alpha_i) \langle \cos(\alpha_i), \sin(\alpha_i) \rangle$$

$$(8.4) \quad s = \sum_{i=1}^n s_i = \sum_{i=1}^n M_i \cos(\alpha_i) \tan(\delta) \langle \cos(\alpha_i), \sin(\alpha_i) \rangle$$

Note that the term cL_i is dropped from (8.4), since the cohesion coefficient c describes molecular attraction among like particles and is zero between soil and a bucket surface. Thus, the safety factor F_s can be defined as

$$(8.5) \quad F_s = \frac{|s|}{|\tau|}$$

When F_s is less than one, sliding of the whole mass along the bucket surface is inevitable. In this case, the total driving force G of the global movement can be computed by

$$(8.6) \quad G = \begin{cases} \tau - s, & \text{if } \tau > 0 \\ \tau + s, & \text{otherwise} \end{cases}$$

In order to simulate the movement of soil mass in a bucket, we decompose G to smaller components which are parallel to the bucket surface. These component forces are distributed to slices so that the dynamics of soil can be considered individually for each slice. After carefully analyzing the behavior of the soil mass, we know that the following constraints must be satisfied:

- 1) The summation of component forces should equal G ;
- 2) All slices should have the same x -acceleration.

The first constraint is obvious. The second one should be always true simply because: 1) a bucket always has a convex shape; and 2) some slices would fall apart and tension cracks or deformation would occur if the x components of their accelerations are different.

Let $G^x = G \cos(\alpha)$ and $G^y = G \sin(\alpha)$ be the x and y components of G respectively, where α is the angle between the vector G and the horizontal. Let g_i be a component force

of G , which is experienced by the bucket surface of i -th slice. From the constraints we have

$$(8.7) \quad G \cos(\alpha) = \sum_{i=1}^n g_i \cos(\alpha_i)$$

$$(8.8) \quad G \sin(\alpha) = \sum_{i=1}^n g_i \sin(\alpha_i)$$

$$(8.9) \quad \frac{g_1}{M_1} \cos(\alpha_1) = \frac{g_2}{M_2} \cos(\alpha_2) = \dots = \frac{g_n}{M_n} \cos(\alpha_n)$$

(8.7)~(8.9) give us $n+1$ equations with $n+1$ unknowns, namely g_1, g_2, \dots, g_n and α . Other variables can be computed according to the geometry of the given configuration. Solving the equations we obtain

$$(8.10) \quad g_i = \frac{M_i \cos(\alpha)}{M \cos(\alpha_i)} G, \quad \text{for } i = 1, 2, \dots, n.$$

$$\text{where } \alpha = \tan^{-1} \left(\frac{1}{M} \sum_{i=1}^n M_i \tan(\alpha_i) \right).$$

Having f_i and g_i computed, we model the soil dynamics in a bucket by using Algorithm 1 to evaluate simultaneous equations in (5.3). In order to do so, we simply replace f_i by $f_i + g_i$ when calculating the rate of changes of each post at the time t_{m+1} . The rest of the algorithm remains unchanged.

9. IMPLEMENTATIONS

9.1 IMPLEMENTATION OF A BULLDOZER

Recall that the terrain surface is represented by a regular tessellation model. An array, namely z , of size $m \times n$ is used to store the height of elevation posts. An element $z(i,j)$ in the array represents the elevation at the location $\langle i,j \rangle$.

As mentioned in section 7, an excavating process of a bulldozer can be separated into three phases. These actions can be simulated by an algorithm with three corresponding stages: digging, piling and soil slipping. First, the algorithm keeps track of the motion of the blade. If the altitude value of the bottom of the blade is denoted by $b(i,j)$ at the location $\langle i,j \rangle$, then any elevation post $z(i,j)$ passed through by $b(i,j)$ are forced to have the same value. This procedure will create a ditch along the path of the bulldozer on the terrain surface.

The second stage models the upward movement of the soil along the blade. Let P be a set of soil prisms which have been passed through by the blade in the last time step. Let $z_p(i,j)$, $z_q(i,j)$ and $z_r(i,j)$ be surrounding posts of a prism $p(i,j)$. The amount of soil contributed by prisms in P to the soil chip moving upwards can be computed by:

$$(9.1) \quad V = \frac{\Delta x \Delta y}{6} \sum_{p(i,j) \in P} \Delta V(i,j)$$

where

$$\Delta V(i,j) = z_p(i,j) + z_q(i,j) + z_r(i,j) - b_p(i,j) - b_q(i,j) - b_r(i,j)$$

Finally, in the third stage the amount of soil computed by (9.1) is put in front of the blade. Since the height that the soil is lifted upward along the blade and the speed in which the soil chips are broken into individual lumps depend on the cohesion property of the given soil, the procedure can be simulated by spreading the soil to a chunk shown below:

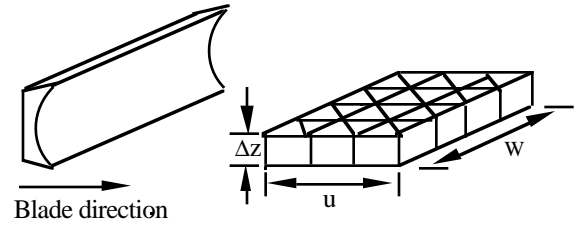


Fig. 13: Dimensions of soil chunk

The dimensions of the soil chunk are determined according to the following equation:

$$(9.2) \quad \Delta z = \kappa (1 + c)$$

$$u = \frac{V}{w \kappa (1 + c)}$$

where V is the total volume calculated by (9.1), w the width of the blade, c the cohesion coefficient, and κ a constant which determines how far forward the soil chip moves during one time step. In the implementation, κ is chosen experimentally to make the simulation looks more realistic.

After all this is done, Δz is added to the elevations of corresponding posts, and the slippage model introduced in previous sections is used to simulate the free flow motion of broken lumps of soil. It should be mentioned that the soil being brought to the top of the berm arrives continuously in the real world. However, with a discrete time simulation process, the chunk is a reasonable representation of the amount and location of the soil that would really arrive during one time step. The slippage model smoothly integrates this chunk into the berm, resulting in a realistic appearance.

Another important phenomena associated with physical properties of soil is swelling, which is due to a number of reasons: 1) the affinity of the soil for water; 2) the base exchange behavior and electrical repulsion; and 3) the expansion of entrapped air within the soil mass [4]. The model simulating the expansion of excavated soil is also discussed and implemented in [9].

9.2 IMPLEMENTATION OF A BUCKET

In implementing a 3-d bucket, we first divide it into $m \times n$ cross sections in a way such that they are parallel to either the x - z plane or the y - z plane. We refer to these sections as x -sections and y -sections respectively. The result of the division is shown in Fig. 14, where an x -section and a y -section are emphasized by two shaded polygons.

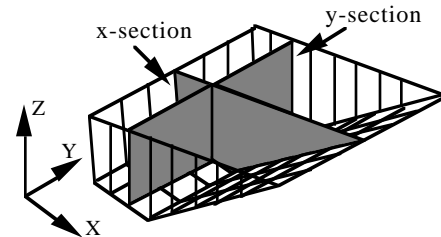


Fig. 14: Dividing a bucket into sections

Therefore, the 3-d soil dynamics in a bucket is reduced to $m \times n$ 2-d cases. For each individual cross section, we further partition a 2-d soil configuration into soil slices (see Fig.

11.). The soil dynamics of each slice is handled by means of the technique introduced in section 8.

A simulation procedure can be described as follows: Each iteration of a simulation can be accomplished by two steps. The first step computes forces for each soil slice of every bucket section according to (5.3) and (8.10). The second step uses the Euler integration method to determine new values for each elevation post (see Algorithm 1). These posts are intersections of x-sections and y-sections.

The cutting and loading activities of a scooploader can be modeled by a method similar to the one presented in section 7. The discussion, therefore, is omitted.

10. CONCLUSION AND FUTURE WORK

Experimental realtime models of a bulldozer and a scooploader have been implemented in the c programming language. Both time and space costs of algorithms are linear in the size of the bulldozer's blade, the size of the bucket and the resolution of the ground mesh. The simulations were done on a Silicon Graphics 4D/240 GTX computer. When using 4 processors, two bulldozers run at 6-8 frames/second. The scooploader model uses 2 processors, running at 10-15 frames per second. The number of elevation posts to model the ground for both models is 90×90 . The simulations look very realistic.

Future research work may include soil compressibility and moisture content. The compression of soil layers is due to deformation and relocation of soil particles and expulsion of air or water from the void spaces [6]. Fundamental principles for estimating settlements of soil under superimposed loading should be explored so it can be used to provide vehicle tracks or conduct trafficability studies. The moisture content of the soil affects its unit weight and cohesion and results in different behaviors. Those properties should be incorporated into analytical models to provide more realistic simulations.

Fig. 15: Two bulldozers are at a work scene

Fig. 16: A scooploader is loading

11. Winston, P. H., *Artificial Intelligence*. Addison-Wesley, pp.75-78, 1984.

Fig. 17: A scooploader is dumping

ACKNOWLEDGMENTS

The authors are very grateful to Dr. Charles E. Hughes and Clay Johnson for revising the paper; to Lance Marrou and Jinxiong Chen for their support.

REFERENCES

1. Balovnev, V.I. *New Methods for Calculating Resistance to Cutting of Soil*. Translated from Russian, Published for the U.S. Department of Agriculture and the National Science Foundation. Washington, D.C., 1983.
2. Bromhead, E. N. *The Stability of Slopes*. Surrey University Press, 1986.
3. Burg, Jeniffer, Moshell, J. Michael, et al., Behavioural Representation in Virtual Reality. *Proceedings of Behavioral Representation Symposium*. Institute for Simulation and Training. Orlando, FL, 1991.
4. Cernica, J. N., *Geotechnical Engineering*. Holt, Rinehart & winston, 1982.
5. Chowdhury, R. N., *Slope Analysis*. Elsevier North-Holland Inc., 1978.
6. Das, Braja M. *Principles of Geotechnical Engineering*. Second Edition, PWS-KENT Publishing Company, 1990.
7. Huang, Y. H., *Stability Analysis of Earth Slopes*. Van Nostrand Reinhold Co., 1983.
8. Kass, Michael and Miller, Gavin. Rapid, Stable Fluid Dynamics for Computer Graphics. *Proceedings of SIGGRAPH '90* (Dallas, Texas, August 6-10, 1990). In *Computer Graphics* 24, 4(August 1992).
9. Li, Xin. Physically-Based Soil Models of Dynamic Terrain in Virtual Environments. *Technical Report*. CS-TR-92-26, University of Central Florida. Nov. 1992.
10. Moshell, J. Michael. Li, Xin. et al. Nap-of-Earth Flight and the Realtime Simulation of Dynamic Terrain. *Proceedings of International Society for Optical Engineering*. Apr. 1990.